Lukas Raffl* and Christoph Holst

Extending geodetic networks for geo-monitoring by supervised point cloud matching

https://doi.org/10.1515/jag-2024-0011
Received January 12, 2024; accepted August 3, 2024;
published online September 10, 2024

Abstract: In this paper we propose a monitoring method that allows the inclusion of point clouds into a geodetic monitoring network. Consequently, network adjustment and a rigorous deformation analysis can be performed allowing consistent error propagation and trustful significance calculation. We introduce a supervised pipeline based on ICP-matching of small-scale laser scan patches. It is specially designed for geo-monitoring applications and allows to improve the spatial resolution as well as the network geometry of monitoring networks in inaccessible hazardous areas in the mountains, where the installation of a sufficient number of targets is difficult. We apply our method to two datasets. The first is a monitoring setup in the laboratory, where we establish the parameters for the supervised patch selection and demonstrate how the network geometry is improved. Second is the real case study of Mt. Hochvogel, where the proposed method helps to clearly improve the spatial resolution of deformation vectors.

Keywords: geodetic monitoring; laser scanning; network adjustment; deformation analysis; ICP matching

1 Introduction

Geo-monitoring is the monitoring of the unbuilt environment. It gains more and more importance and has already become an indispensable part of risk prevention in the Alps and other mountainous regions. Due to climate change and the accompanying more extreme weather conditions, the number of gravitational mass movements like landslides and rockfalls in the Alpine region has increased [1]. In combination with growing urbanisation in the mountains, this raises the risk of disastrous events for local communities and infrastructures. Therefore, risk prevention is a key challenge for our society in the near future. Geo-monitoring systems, including geotechnical and geodetic sensors, are favourable alternatives or additions to large and expensive protection structures and allow to better understand the ongoing geological processes and forecast eventual events. In geo-monitoring, we usually want to know

- Where do we have deformations?
- How large are the deformations?
- And in which direction is the object moving?

However, we have to deal with some challenges. Especially in the case of rockfalls, the movements are typically very small. Still, an early detection is desired so that a warning can be launched as early as possible. On the other hand, no false alarms must be given in order not to lose the acceptance of the people. Consequently, the goal of an early warning system is to provide 3D deformation vectors with high accuracy, high reliability and high spatial coverage.

Today different instruments and methods for geo-monitoring are available, providing different characteristics in terms of temporal resolution, spatial resolution and measurement accuracy. Geotechnical sensors like wire extensometers measure precise distance changes with a high temporal resolution, even in real-time. Geodetic measurement instruments like Global Navigation Satellite System (GNSS) receivers and tacheometers, on the other hand, are capable to determine 3D deformation vectors including the displacement direction and magnitude. By creating a geodetic monitoring network consisting of a number of signalised monitoring points, the hybrid network measurements (GNSS and tacheometer) can be evaluated within a rigorous deformation analysis [2]. Due to the redundancy within the point networks, realistic uncertainty information about the results can be calculated and the significance of deformations can be statistically tested. However, these point-wise measurement methods are limited to a number of preselected points, which are usually difficult to install within the hazardous area. Thus, local, small-scale processes may be missed, because of a lack of areal coverage.

For a high spatial resolution, area-based measurement technologies like terrestrial laser scanning (TLS), airborne

***Corresponding author: Lukas Raffl**, Chair of Engineering Geodesy, TUM School of Engineering and Design, Technical University of Munich, 80333 Munich, Germany, E-mail: lukas.raffl@tum.de.
https://orcid.org/0000-0002-9425-1905
Christoph Holst, Chair of Engineering Geodesy, TUM School of Engineering and Design, Technical University of Munich, 80333 Munich, Germany, E-mail: christoph.holst@tum.de. https://orcid.org/0000-0002-7966-4322

laser scanning (ALS), photogrammetric techniques as well as spaceborne and ground-based differential synthetic aperture radar interferometry (DInSAR) can be used. Even more monitoring techniques are frequently used, but should not be addressed here.

TLS and areal deformation analysis have already become established in geodetic monitoring [3–5]. Due to the reflectorless scanning technology and the dense sampling of the entire surface within the selected scanning resolution, inaccessible areas can also be included and deformations can be detected even in areas where they may not have been suspected [6]. However, using point clouds for geo-monitoring raises new challenges [7, 8]. Besides others, a major challenge is the absence of identical points across the different measurement epochs. Several approaches have been developed to calculate deformations from two point clouds nevertheless (see Section 2.2), but still a statistical congruency test based on identical measurement points is only possible in a few cases [9]. Also, it is still not possible to combine point-wise and areal measurements in a hybrid evaluation.

We pursue a novel monitoring approach that allows us to integrate point cloud data into a conventional rigorous deformation analysis. Our workflow is specifically developed for geo-monitoring applications where an increased number of precise 3D vectors, including significance information, is required, but not all network points can be marked. In this paper, we describe our monitoring approach, which allows us to:

- Create additional virtual network points from point cloud patches using ICP matching
- Filter unsuitable virtual points using “supervised” ICP matching
- Increase the spatial resolution and improve the network geometry by integrating the virtual points into the network adjustment
- Evaluate our novel approach in the laboratory and on a geo-monitoring application (Mt. Hochvogel)

In Chapter 2, we will discuss and compare different approaches to derive deformation values within geodetic monitoring based on the sensors and evaluation methods used. In Chapter 3, we will then present our proposed workflow of supervised point cloud matching, introducing all the steps needed to transition from point clouds to an extended geodetic network. The validation of our method, using two applications, is then described in Chapter 4. The results are discussed in Chapter 5 before ending the article with a conclusion and outlook in Chapter 6.

2 Geodetic monitoring

The aim of geodetic monitoring is to determine geometrical deformations in shape or position of an object between two measurement epochs [10]. Besides the quantification of geometric changes, also the identification of its statistical significance based on the measurement uncertainties is a major part of the deformation analysis in engineering geodesy [11]. With different measurement techniques, also different evaluation methods are used. Point-wise geodetic measurements are typically combined into a geodetic network where gross measurement errors can be identified and the same points are measured in every epoch. On the other hand, using TLS as an area-based measurement method the outcome is a point cloud for each epoch. Deformations can be derived by the comparison of two point clouds. A special case of point-cloud-based monitoring is patch-based monitoring where single point cloud patches are evaluated separately and a more point-wise characteristic in the deformation analysis occurs. In the following those three monitoring approaches, network-based (Section 2.1), point-cloud-based (Section 2.2) and patch-based monitoring (Section 2.3), are introduced and the benefits and limitations of each for geo-monitoring are discussed.

2.1 Network-based monitoring

Using a geodetic network consisting of measurements to selected and signalised single points is the conventional approach in geodetic monitoring [10]. Based on the observation of identical points in each epoch, a rigorous deformation analysis including statistical significance tests can be performed. Hereby, the calculated deformation values are tested to determine whether they are statistically significant or not relative to the accuracy of the point determination and based on the selected confidence level [2]. The network consists of a set of discrete (i) control points, which are assumed to be stable, and (ii) object points, located in the moving area characterising the deformation process. Creating a network structure of geodetic measurements between the points leads to redundancy and ensures a realistic uncertainty estimation for the determined point coordinates. In each epoch, the identical point field is observed and evaluated in a free network adjustment. If the variances of the two measurement epochs are comparable, point deformations are calculated and localised according to the congruency model. The congruent control points define the datum and thus the coordinate system for the deformation

analysis, whereas some control points may also be eliminated and added to the set of object points as they are detected unstable. As a result, the 3D displacement vector for each object point (including eliminated control points) and its proof of significance is determined.

However, when performing network-based monitoring, the deformation process is generalised by a number of object points. Prior assumptions about the deformation process have to be made in order to select representative points. The limited spatial resolution also limits the detailed modelling and understanding of the deformation process.

2.2 Point-cloud-based monitoring

Instead of discretising the deformation area by a number of carefully selected and signalised points, the surface geometry of the whole area can be represented by a dense point cloud with a high spatial resolution captured by TLS. The main challenge in comparing two point clouds is overcoming the problem of missing identical points across the two epochs. This is because the scanning raster is not reproducible in the different epochs, especially not if the object surface has changed between the epochs due to deformations and thus, the measurement points will not fall strictly on the same locations. Nevertheless, various methods have been developed for deriving deformations from two point clouds. According to ref. [7], the different approaches can be grouped into three categories: point-cloud-based, point-based and parameter-based strategies. Not all methods should be addressed here, but some are mentioned in the following.

Point-cloud-based approaches usually use the complete point clouds of both epochs to determine changes between them. The result is often a colour-coded heat map which depicts the magnitude of geometrical differences between the two point clouds. The comparison is either based on the point cloud itself, like in the M3C2 algorithm [12, 13] or on best-fitting surfaces from triangulation [14, 15] or free-form parametrisation [16].

Parameter-based methods approximate the point cloud or parts of it using analytical surfaces like geometrical primitives [17–20]. Deformations are then identified analysing changes in the estimated parameters.

Point-based strategies reduce both point clouds to a number of identical points, which then can be compared directly across the epochs. Comparable points are created by reducing and interpolating the irregular point clouds to a specific grid [21], by estimating and intersecting planes [22] or by extracting feature points based on machine learning [23] or on additional RGB images [24]. Furthermore, features can be extracted from the 2D representation of a digital terrain model (DEM) created from the laser scans for each epoch [25, 26].

In geo-monitoring, mostly point-cloud-based and point-based strategies are used as natural objects are difficult to describe by geometric primitives. However, only point-based strategies result in actual 3D deformation vectors (magnitude and displacement direction). Other approaches have to accept a loss in dimension because, in most cases, only one-dimensional offsets between surfaces, hence in the direction of the local surface normal, are calculated. Moreover, it should be mentioned that a precondition for most of the methods is that the two point clouds are already located in the same coordinate system. Therefore, an accurate point cloud registration over two epochs is another challenge in point-cloud-based monitoring, because registration errors later directly add to the actual displacement values [27].

2.3 Patch-based monitoring

A special case of point-cloud-based monitoring involves subdividing the point cloud into tiles or even using only selected patches [28–30]. In this case, a rigid body movement is calculated individually for each point cloud patch, for example, using the iterative closest point (ICP) algorithm [31]. This process is known as ICP matching. Although the number of object points and thus the spatial resolution is reduced in comparison to other point-cloud-based strategies, ICP matching gives an actual 3D vector for each patch [32] and the patches can even be seen as virtual target points [22, 33].

Using patches makes the deformation analysis more resistant to measurement noise depending on the number of scan points per patch. However, even for point-based strategies where identical points are created between epochs, the proof of statistical significance remains challenging due to the unknown accuracy information of the derived points. Given the numerous influences on measurements and ICP matching, a precise estimation of the stochastic model is nearly impossible. Therefore, we propose a novel monitoring strategy combining network-based monitoring and patch-based monitoring.

3 Methodology of supervised point cloud matching

In the following section, we outline the workflow for supervised point cloud matching, a methodology particularly designed for scanning total stations but also adaptable to point clouds obtained from laser scanners or photogrammetry (Figure 1). The fundamental idea is to create

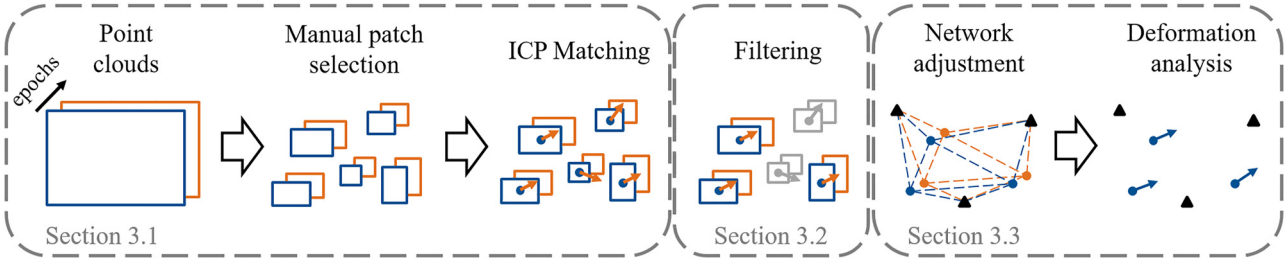

Figure 1: Workflow of extending geodetic monitoring networks by the proposed supervised point cloud matching.

corresponding virtual target points from laser scan patches using ICP matching and subsequently converting these target points into polar single-point observations. These observations can then be integrated into a free network adjustment and a rigorous deformation analysis [34].

Herein, it is essential that the patches are suitable for ICP matching. Therefore, we introduce a supervised selection of patches where each chosen patch is checked for suitability.

In this workflow, we assume, as a simplification, that all point clouds are already registered. However, this is not a mandatory requirement for the method, but it makes it easier to find homologous patches. Nevertheless, the ICP needs at least a rough alignment in order to converge to the correct solution. Although the initial alignment influences the transformation parameters of the patches, it is not relevant later as the actual datum definition comes from the network adjustment. If a sufficient number of virtual point pairs is identified in areas assumed to be stable, these pairs can be employed for fine registration.

In the following the three steps of the proposed workflow are described. First, in Section 3.1 the creation of virtual target points using ICP matching is explained. In Section 3.2 we introduce the supervised selection of suitable patches based on a Monte Carlo (MC) simulation. Finally, in Section 3.3 the integration of the filtered, virtual observations into the network adjustment and rigorous deformation analysis is described.

3.1 Virtual targets from ICP matching

The ICP algorithm determines the 3D transformation parameters between two point clouds of the same patch P. In case the two point clouds were captured in two different measurement epochs k, the parameter set can be used to transform any point from the first epoch $k = 0$ to a follow-up epoch $k > 0$. Based on this concept, for each patch P_i a virtual target $\mathbf{P}_i$ is created in all epochs k (Figure 2a):

1. Define virtual point $\mathbf{P}_{i,0}$ in zero epoch. We use the patch's centroid as the virtual point, but any other point can also be chosen.
2. Determine transformation $\mathbf{T}_{i,k}$ between zero epoch and epoch k using ICP

$$\mathbf{T}(\mathbf{t}|\mathbf{R})_{i,k} = \mathrm{ICP}(P_{i,0} \rightarrow P_{i,k}) \tag{1}$$

3. Transform virtual point $\mathbf{P}_{i,0}$ into epoch $k \rightarrow$ updated virtual point $\mathbf{P}_{i,k}$

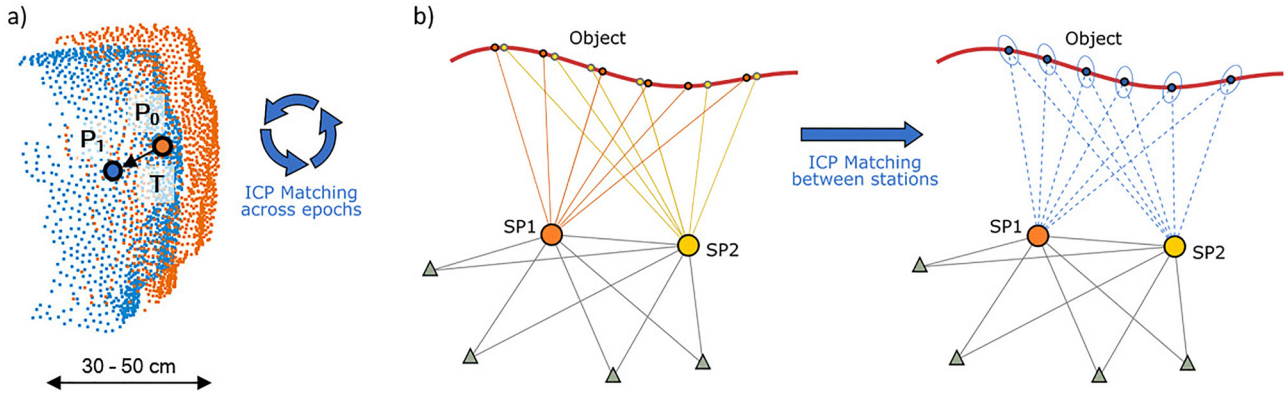

Figure 2: Procedure for creating corresponding points using ICP matching (a) across two epochs and updating the virtual point, and (b) between two stations and integrating them into the geodetic network consisting of control points (triangles) and object points (circles).

$$\mathbf{P}_{i,k} = \mathbf{T}(\mathbf{t}|\mathbf{R})_{i,k}\mathbf{P}_{i,0} \tag{2}$$

Given that the ICP algorithm determines the rigid body transformation between two point clouds, our workflow assumes there are no deformations within one patch. Typically, we use manually selected point cloud patches with a size of approximately 30–50 cm, depending on the surface structure.

The ICP matching cannot only be performed across two epochs but also between two stations (Figure 2b). If the same patch is scanned from two different stations within the same epoch, ICP matching can be used to create redundant observations. The procedure remains the same: the virtual point of the reference patch is transformed into the point cloud of the second station using the transformation parameters determined by ICP. The resulting redundant single-point observations of the patches improve the overall network geometry and, thus, the accuracy of the points (see Section 3.3).

However, despite different viewing angles on the patch, the ICP still has to give reliable and correct results. Regarding the network geometry, it is desirable to have very different viewing angles on the object, but for ICP it is better to have a very similar viewing angle. This may cause that not for all patches redundant observations can be created.

3.2 Supervised selection of structures

The quality of the ICP result depends on different factors [35], especially the measurement configuration, patch geometry, measurement noise and scan resolution. Consequently, for each patch has to be checked if – in case of an arbitrary deformation – the matching is (i) unambiguous and (ii) reproducible. Both conditions are primarily influenced by the structure's geometry:

1. A lack of geometric variation within the structure leads to the matching being inaccurate in certain directions, for example in the case of a (quasi) planar structure (Figure 3b).
2. Repeating geometries within the structure lead to several local minima to which the ICP converges, depending on the occurring displacement (Figure 3c).

To achieve unambiguous and thus reproducible matching the selected patch has to have a certain geometric variation (Figure 3a). Only structures that allow reproducible matching in all three dimensions should be used. In other words, the ICP should always converge to the exact same local minimum, independent of a possible rigid-body movement between two epochs. Verification can be done either analytically, by analysing the structure's geometry, or statistically in a simulation.

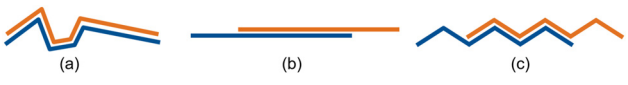

Figure 3: Example of a (a) suitable, (b) ambiguous and (c) repeating geometry for ICP.

Using the second approach, besides the geometry also other factors contribute to the result, for example the scan resolution [36]. Hence, we perform a MC simulation for each patch pair P_i and P_j that is matched.

Within the MC simulation, the ICP matching is repeated n times for the same patch pair. After an initial alignment of the point cloud pair, in each iteration m the patch P_j is moved by a certain displacement $\mathbf{d}_m$ relative to the reference patch P_i.

$$\mathbf{d}_m = \begin{bmatrix} \Delta x_m \\ \Delta y_m \\ \Delta z_m \end{bmatrix} \tag{3}$$

$$P'_{j,m} = \mathbf{T}(\mathbf{d}_m|\mathbf{0})P_j \tag{4}$$

The maximum displacement is limited by a bounding box (Figure 4). Within this bounding box, n uniformly distributed displacements are randomly created.

Each moved patch $P'_{j,m}$ is then matched on the reference patch P_i using the ICP algorithm.

$$\mathbf{T}(\mathbf{t}|\mathbf{R})_m = \mathrm{ICP}\left(P'_{j,m} \rightarrow P_i\right) \tag{5}$$

As already emphasised, the ICP should always convert to the same minimum and thus the initial registration result. The deviation between nominal displacement $\mathbf{d}_m$ and translation $\mathbf{t}_m$ given by the ICP matching is the registration error $\mathbf{e}_m$

$$\mathbf{e}_m = \mathbf{d}_m + \mathbf{t}_m \tag{6}$$

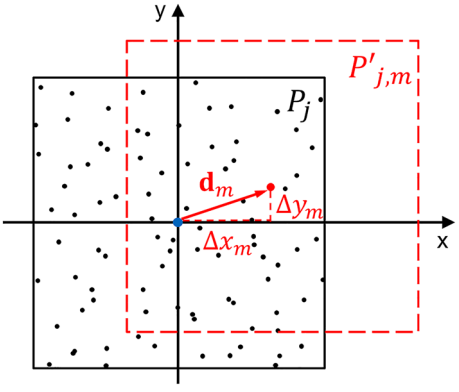

Figure 4: Principle of the MC simulation in 2D. The second point cloud is successively moved to a number of uniformly distributed starting points within a predefined box and the ICP is performed.

The variation of $\mathbf{e}$ over all iterations m can be taken as a measure for the matching precision $\mathbf{u}_{i,j}$.

$$\mathbf{u}_{i,j} = \begin{bmatrix} u_x \\ u_y \\ u_z \end{bmatrix}_{i,j} = \max(\mathbf{e}) - \min(\mathbf{e}) \tag{7}$$

For suitable patches $\mathbf{u}_{i,j}$ is expected to be small. However, depending on the geometry, a certain variation in the registration is expected. Thus, a suitable threshold $u_{\max}$ for the registration precision within the MC simulation has to be defined (see Section 4.1), whereby all elements of $\mathbf{u}_{i,j}$ must be below the threshold value $u_{\max}$. Selected structures that do not fulfil this condition can be eliminated.

The point clouds may be captured from the same station in two different epochs, from two different stations within the same epoch, or even from two different stations in two different epochs. The MC simulation evaluates the actual point clouds later used in the ICP matching. Consequently, the analysis evaluates not only the patch geometry but also the actual measurement configuration, measurement noise, and scan resolution. However, since these latter parameters remain constant throughout the MC simulation, all point cloud pairs P_i, P_j of the same structure must be analysed individually. The box size should be chosen according to the expected displacement to ensure the patch is unambiguous within the border of a maximal expected movement.

An example of supervised structure selection is shown in Figure 5. In this case, a boulder was scanned and the point cloud was divided into rectangular patches with a size of approx. 30 cm by 30 cm. After deformation, the boulder was scanned again and the exact same grid was placed over the point cloud, albeit with a slight shift in grid position relative to the object due to the movement. Nevertheless, the patches can be considered homologous, given that the movement is significantly smaller than the patch size. ICP matching gives a deformation vector for each patch. As the monitoring object is one solid rock, it can be expected to move homogeneously, resulting in similar deformation vectors across all patches. However, Figure 5b reveals several outliers in the results. These can be attributed to a lack of geometric variation in certain patches. The MC simulation can eliminate all unsuitable patches (Figure 5c). In this case, a threshold value of $u_{\max} = 1\,\text{mm}$ was employed. Ultimately, the vectors of the remaining patches (highlighted in green) show a homologous movement pattern.

In contrast to comparable methods, such as feature-based approaches, which often use histograms to filter out false results [26], our proposed method allows for the examination of expected result quality prior to the actual calculation.

3.3 Network adjustment and rigorous deformation analysis

After unsuitable patches have been rejected, still no realistic uncertainty information for the remaining virtual points is available. In the context of point-based monitoring, geodetic network measurements and adjustments allow the most consistent error propagation and, thus, a comprehensive significance calculation. Consequently, the virtual points are converted into tacheometric pseudo observations $\mathbf{l}_{i,k}$, each consisting of horizontal angle Hz, vertical angle V and slope

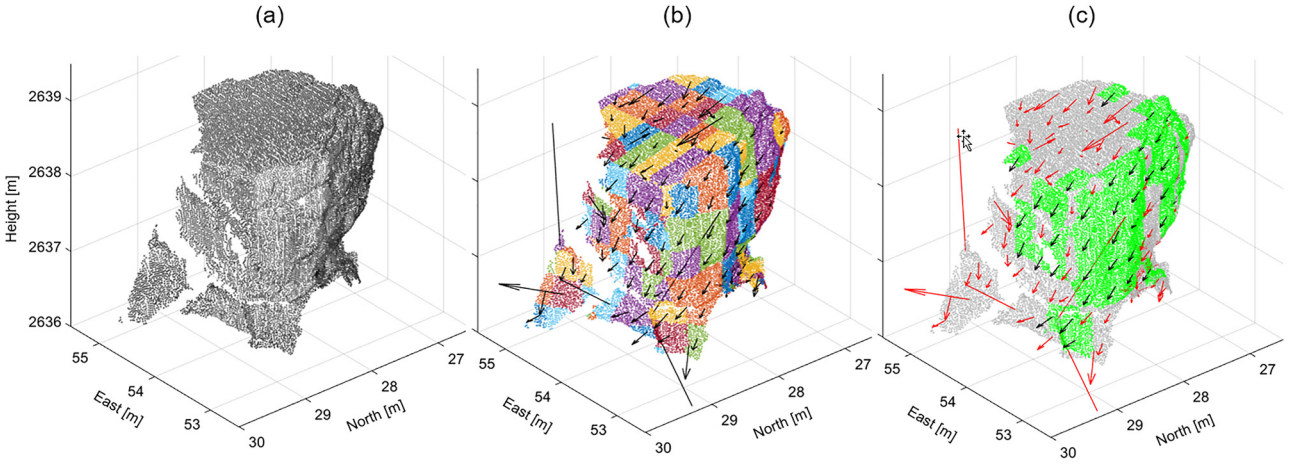

Figure 5: Example for supervised structure selection on a boulder: (a) laser scan of the rock captured in two epochs, (b) random tiling of the block and resulting deformation vectors using ICP matching and (c) filtered patches after the MC simulation.

distance S

$$\mathbf{l}_{i,k} = \begin{bmatrix} Hz \\ V \\ S \end{bmatrix}_{i,k} = \begin{bmatrix} \arctan(\Delta x/\Delta y) \\ \arccos(\Delta z/S) \\ \sqrt{\Delta x^2 + \Delta y^2 + \Delta z^2} \end{bmatrix}_{i,k} \tag{8}$$

where Δx, Δy and Δz are the coordinate differences between the virtual point and measurement reference point of the instrument. Finally, all pseudo observations of the same epoch k can be combined with other single-point measurements from the total station or GNSS and evaluated in a free network adjustment. At the end not only adjusted coordinates $\hat{\mathbf{x}}$ for all observation points result, but also the corresponding covariance matrix $\mathbf{\Sigma}_{\hat{\mathbf{x}}\hat{\mathbf{x}}}$ containing precision information for each point.

Besides the observation accuracy, the uncertainty of the adjusted points is also influenced by the network design. Generally, a higher redundancy improves the reliability and controllability of the network, thereby leading to higher quality. A measure for the controllability of each observation and thus the probability of identifying possible gross errors are the partial redundancies r_i. If within the network adjustment a global test is performed to ensure that the variance factor *a priori* equals the variance factor a posteriori $\left(\sigma_0^2 = s_0^2\right)$, the partial redundancies r_i can be derived from the diagonal elements of the redundancy matrix according to

$$\mathbf{R} = \mathbf{\Sigma}_{vv}\mathbf{\Sigma}_{ll}^{-1} \tag{9}$$

with the covariance matrix of the corrections $\mathbf{\Sigma}_{vv}$ and the covariance matrix of the observations $\mathbf{\Sigma}_{ll}$. A partial redundancy of $r_i = 0$ indicates an uncontrolled observation, while a value of $r_i = 1$ reflects full controllability. By comparing the partial redundancies, the benefit of additionally included pseudo observations on the network design can be examined.

Point deformations between two epochs $k - 1$ and k are then typically calculated based on the congruency model [2]. This requires the presence of corresponding points in both epochs in order to calculate coordinate differences $\mathbf{d}$ and the corresponding covariance matrix of the differences $\mathbf{\Sigma}_{\mathbf{dd}}$.

$$\mathbf{d} = \hat{\mathbf{x}}_k - \hat{\mathbf{x}}_{k-1} \tag{10}$$

$$\mathbf{\Sigma}_{\mathbf{dd}} = \mathbf{\Sigma}_{\hat{\mathbf{x}}\hat{\mathbf{x}},k} + \mathbf{\Sigma}_{\hat{\mathbf{x}}\hat{\mathbf{x}},k-1} \tag{11}$$

The global congruency test is then checking if deformation are statistically significant

$$T_{\mathbf{d}} = \frac{\mathbf{d}^T\mathbf{\Sigma}_{\mathbf{dd}}^{-1}\mathbf{d}}{\operatorname{rank}(\mathbf{\Sigma}_{\mathbf{dd}})} \geq F_{\operatorname{rank}(\mathbf{\Sigma}_{\mathbf{dd}}),r,1-\alpha} \tag{12}$$

with the testing value $T_{\mathbf{d}}$, the threshold F of the Fisher distribution, the redundancy r of the network and the significance level α.

4 Experimental validation

For validation, the proposed method is applied to two applications. Firstly, a constructed setup in the laboratory is used (Section 4.1) to

- evaluate the filtering by MC simulation and find a suitable threshold $u_{\max}$,
- analyse the improvement of the network geometry, and
- compare the results to reference measures on prisms.

Afterwards, the method is applied to the rockfall monitoring on Mt. Hochvogel (Section 4.2), providing an opportunity to assess the performance of the extended network approach in a real-world scenario. In both applications, a Leica Nova MS60 scanning total station is used. Single-point measurements and point clouds are acquired using the same instrument and within the same instrument coordinate system.

4.1 Laboratory setup

A small monitoring network was established in the laboratory (Figure 6). It consists of four stable control points and ten moved object points. All object points are installed on a board that can be moved horizontally and thus create displacements. A combination of signalised and non-signalised target points was used. Standard round prisms, mini prisms and reflective tapes are common target signalisations and give reference values for the displacement. Furthermore different structures can be found on the board, suitable for the proposed ICP matching approach. Some elements (white corners) have a more flattering geometry for ICP than others (stones). The scanning of all structures gives a total of six scan patches for ICP matching. Patch 316 is intentionally chosen to be ambiguous for ICP. The points 101–104 are stable and used as datum points in the deformation analysis.

In all epochs, all targets and patches are measured/scanned from two stations (201 and 202). The point clouds have a resolution of 3 mm on the object. After measuring the zero epoch, the board is moved four times and each time a follow-up epoch is measured. The first two movements are carried out in x-direction, perpendicular to the line of sight of the two instrument stations. The board is moved by approx. 1 cm each time. The second two movements then are in y-direction, in line of sight. Again, the magnitude of the displacement is approx. 1 cm each.

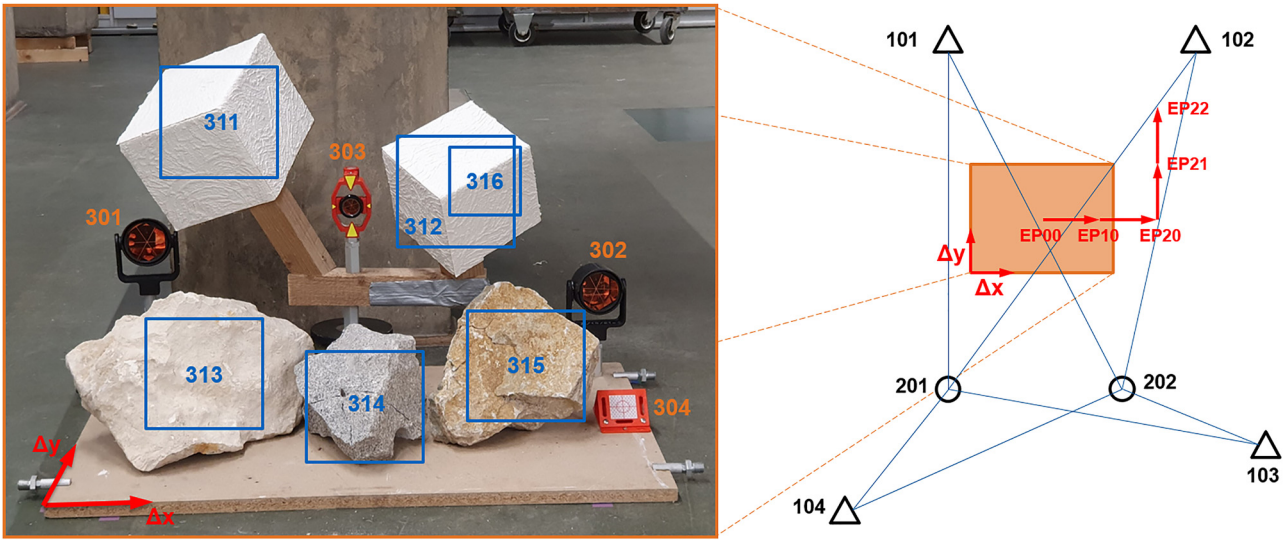

Figure 6: The setup in the laboratory consists of a number of reflectors and scannable objects on a board. Deformations are induced by moving the whole plate.

However, the results of all four epochs showed a similar accuracy, independent of which direction the displacement occurred. Thus, in the following, we only show the result of the deformation analysis between the zero epoch (EP00) and the last follow-up epoch (EP22), in which we have movements in both directions.

First, the MC simulation is performed for each patch. Especially for the rock faces it is not clear if all of them are suited for ICP matching. As the maximal movement in x and y is about 2 cm each, the used box size for the simulation is 5 cm to cover the full range of expected movement within the simulation. Figure 7 shows the results of the simulation for a corner (311), a rock face (313) and an edge (316). As expected, the edge geometry (316) is ambiguous for the ICP along the edge and the patch has to be eliminated. The resulting precision of the corner geometry, on the other hand, is very good. The rock face, however, shows some variation in the matching result, but it is smaller than the nominal observation accuracy of the instrument. All other patches deliver a very high precision as well, similar to patch 311.

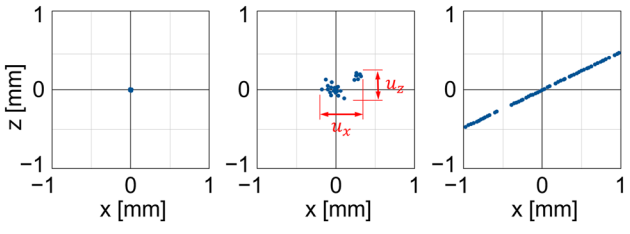

Figure 7: Result of the MC simulation for the patches 311 (left), 313 (center) and 316 (right).

In the following we assume that with a filtering threshold similar to the measurement accuracy of the instrument, a high network accuracy is secured. Meaning, that no observations with an accuracy way worse than the existing total station observations are included. Thus, a threshold

$$u_{\max} = 1\,\text{mm} \tag{13}$$

is selected. Consequently, only patch 316 has to be eliminated in the present case.

Next step is the free 3D network adjustment [37]. To investigate how the network quality can be improved by the additional targets, the partial redundancies are evaluated. However, the network geometry in the laboratory setup is already very good. Therefore, additional observations do not bring any decisive improvement. In many applications, however, the network design is limited due to the measurement environment and there is potential for improvement. For this reason, the network design is also degraded in the laboratory to show that, in this case, the virtual observations lead to an improvement. Only two of the four datum points (101, 103) and only one of the four reflectors (303) on the board are used. Figure 8 shows the resulting network configuration in the zero epoch.

Afterwards, the network is extended by the observations to the five remaining patches. Figure 8 depicts the partial redundancies of the horizontal angle observations for both configurations. In the extended configuration, not only do the additional included observations have a high

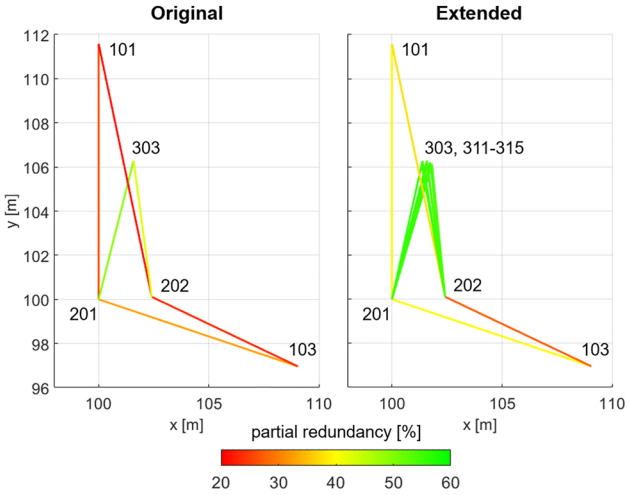

Figure 8: Partial redundancies of the horizontal angle (Hz) observations for a low number of object points (left) and a high number of object points (right).

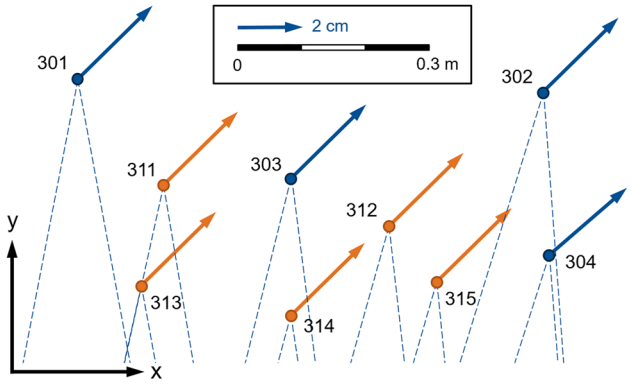

Figure 9: Resulting deformation vectors for the reflectors (blue) and remaining patches (orange). Total station measurements are shown as blue dashed lines.

partial redundancy, but the partial redundancy of the already existing observations is also improved.

The improvement can also be seen in Table 1 where for each observation type the average partial redundancy is listed. The biggest improvement is made in the distance observations, while the other two groups also show a large improvement. As the measurement conditions in the laboratory are ideal, the point accuracies are with about 0.1 mm standard deviation already very high for the configuration without patches. Therefore, no improvement could be seen in the point accuracies itself.

Finally, the deformation vectors between the two epochs are calculated for the full network configuration and depicted in Figure 9. All vectors show the same magnitude and direction of movement. If not known, it cannot be distinguished between a marked point or a virtual target from a laser scan. The accuracy of the virtual points is similar to the accuracy of the marked points and again it is in the range of 0.1 mm. The point with the worst accuracy (0.2 mm) is point 304, marked by a reflective tape.

This is a first proof that the proposed method works. It also confirms that the chosen threshold for filtering unsuited patches is appropriate as the remaining patches delivered correct results. As already addressed in Section 3.2, the quality of the ICP result is not only affected by the patch geometry but also by the scan resolution.

To create a worse scenario, in each epoch all patches are also captured with a resolution of 6 mm. In this case, the resulting ICP precision for patch 313 is above the threshold and also other patches have to be eliminated. If not, the network accuracy gets worse and the resulting deformation vectors for those virtual points do not match the nominal movement given by the reflectors. This confirms as well that the threshold of 1 mm is well suited.

Table 1: Average redundancy components.

	Original	Extended
#Points	5	10
Redundancy	5	20
Σr_{Hz}	2.0	8.1
Σr_V	2.0	7.0
Σr_S	1.0	4.9
avg (r_{Hz})	32.6 %	50.5 %
avg (r_V)	33.5 %	43.8 %
avg (r_S)	17.2 %	30.8 %

4.2 Study area Mt. Hochvogel

Mt. Hochvogel is the highest peak in the Allgäuer Alps, located on the German-Austrian border (Figure 10). It is exposed to strong erosion and characterised by brittle, tectonically stressed and fissured main dolomite, making it prone to rockfalls and other natural hazards. Over the past decades, an enormous cleft has formed right on the summit, splitting the entire mountain top into two parts. The southern part threatens to break off completely and fall down on the Austrian side, with an estimated volume of up to 260,000 m^3. By now, the main crack extends over a length of about 35 m in SW-NE direction and is already gaping more than 5 m at its widest point, while several smaller crevices are showing high opening rates as well, making the modelling of the failure process more complicated. The increasing number of extreme weather events, caused by

Figure 10: The summit of Mt. Hochvogel (2,592 m a.s.l.), located on the German-Austrian border, with its enormous cleft. The southern part (left part in the image) is moving several mm per month and threatens to break off completely.

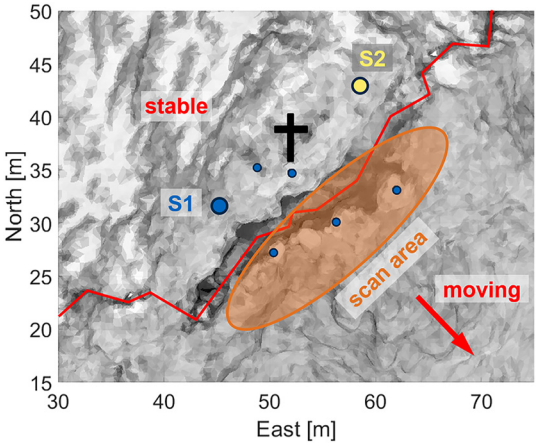

Figure 11: Measurement setup on Mt. Hochvogel and marked points (blue circles) that were measured from both stations (S1, S2).

climate change, further accelerates the failure process and increases the likelihood of rockfalls.

To better understand the present failure process and to implement an early warning system, several measurement systems were set up on the mountain including a geodetic monitoring network based on total station and GNSS measurements [38]. Additionally, terrestrial laser scans of the main crack are captured using the scanning total station.

In this work, our emphasis is on the total station network and on the examination of the network improvement by extending it by virtual targets derived from laser scans. The total station network comprises marked points located on both the stable and moving parts of the summit (see Figure 11). However, not all marked points are visible from both stations, thereby not increasing the redundancy of the network. Figure 11 illustrates only those marked points that are measured from both stations.

The first laser scans were captured in September 2018, followed by a second epoch in July 2019. In both epochs, the main crack was scanned from two stations with a large overlap in the scans (Figure 11). Using a scanning total station the scan resolution, however, is limited. The average scan resolution in both epochs is about 1 cm. As discussed in the previous section, a lower scan resolution makes it harder to find suitable patches.

The goal was to find patches that were scanned from both stations in order to generate redundant observations later. For that, a patch that is selected in the scans from both stations is immediately evaluated with the MC simulation. Again, a threshold of 1 mm is used, as the movement of the southern side of the summit is small and thus the accuracy requirement is high. However, due to the variation of the viewing angles on the object by up to 90° between the two stations (see Figure 11) and the limited area of overlap, ICP matching between the stations fails for many patches. Consequently, some of the virtual targets are observed by only one station. In the end, a total of 24 patches were manually extracted from the scans (Figure 12). For example, individual boulders where no internal deformation is to be expected.

Next, the ICP quality is also checked between homologous patches of both epochs. As the number of points that are only observed from one station is high, this filtering step is crucial. Redundancy-free observations have a partial redundancy of $r_i = 0$ and are not controlled by other observations. Thus, a possible gross error within the ICP matching cannot be detected in the network adjustment, inevitably leading to a wrong result in the deformation analysis. However, the MC simulation can minimize this risk. As a result of the MC simulation, three patches were rejected, as they are not suited for reliable matching. The visual analysis of the rejected patches revealed changes in their inner geometry due to erosion. In this case, the ICP matching is no longer reliable.

After calculating the virtual targets for the remaining 21 patches, pseudo observations are generated. Since the scanning total station was used to carry out additional network measurements, the pseudo observations are added to these. Thus, the number of object points in areas that are difficult to access is significantly increased by the additional virtual targets derived from laser scanning, and the spatial resolution is improved.

Also, the overall network configuration is improved. Due to the limited accessibility on Mt. Hochvogel, the design of the monitoring network is not ideal. However, the additional target points help to improve the network

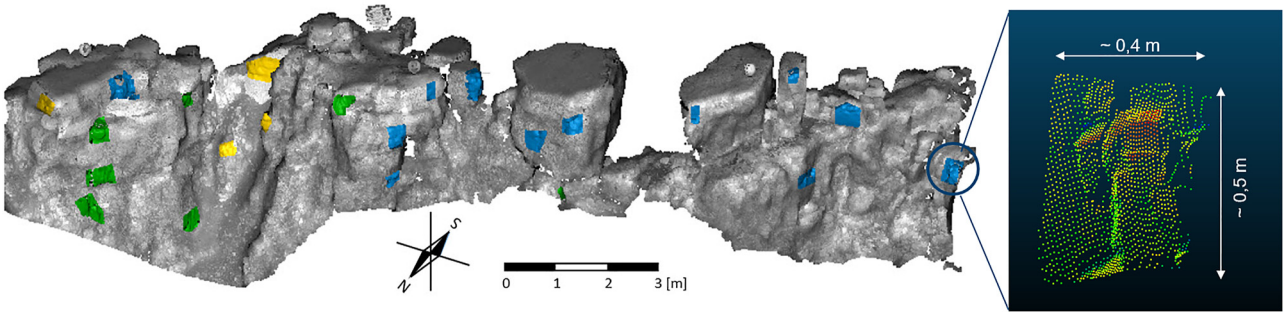

Figure 12: Point cloud of the southern, moving part of the cleft and manually selected patches (blue: station 1, yellow: station 2, green: both stations).

Table 2: Average redundancy components.

	Original	Extended
#Points	30	51
Redundancy	20	50
Σr_{Hz}	4.5	14.5
Σr_V	7.0	17.0
Σr_S	8.5	18.5
avg (r_{Hz})	12.4 %	21.6 %
avg (r_V)	19.5 %	25.4 %
avg (r_S)	23.8 %	27.7 %

quality. Again, the partial redundancies before and after extending the network by virtual observations are analysed (Table 2).

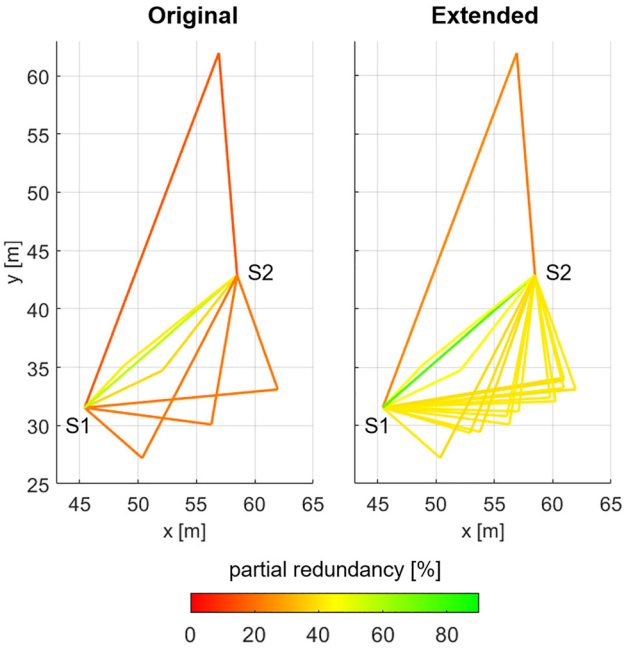

Figure 13: Redundancy component of the horizontal angle (Hz) observations for the original network (left) and after including the virtual points (right).

The average improvement, however, seems to be small. This can be explained by the large number of points that are observed from only one station and thus do not raise the redundancy of the network. As their partial redundancy $r_i = 0$, the average partial redundancy of the observations is still quite small. The improvement can clearly be seen in Figure 13, where only the observations with partial redundancy $r_i > 0$ are shown. All observations with a partial redundancy of $r_i = 0$ are not depicted.

Finally, the rigorous deformation analysis is performed. The horizontal components of the resulting 3D deformation vectors are shown in Figure 14. Between September 2018 and July 2019, the gap opened by around 21 mm in horizontal direction. In vertical direction, almost no movement happened. The virtual points from the patches (orange points) give the same results as the marketed points (blue points), both in direction and magnitude. This confirms the functionality of the method also in a real use case.

Furthermore, the enhanced spatial resolution enables the detection of more details regarding the movement. For

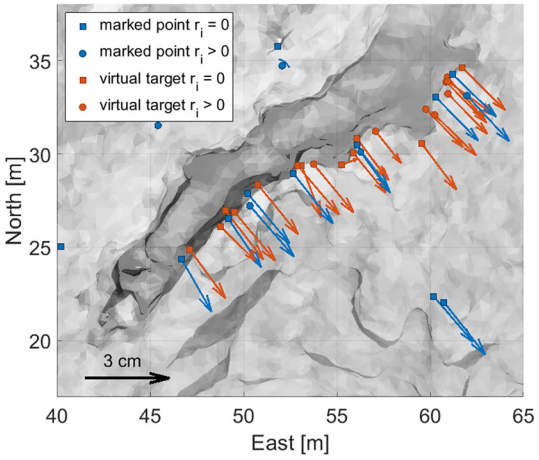

Figure 14: Horizontal component of the resulting deformation vectors between September 2018 and July 2019.

Table 3: Average standard deviation of the deformation vectors.

	Original	Extended
#Points	19	40
σ_x [mm]	2.0	1.8
σ_y [mm]	1.8	1.8
σ_z [mm]	1.8	1.4

example, the additional targets uncovered that a specific block, located at approximately 55 m East and 29 m North, is moving differently, ultimately leading to its collapse in 2021.

The average standard deviation of the deformation vectors is less than 2 mm and could also be slightly improved by adding the virtual targets (Table 3). All detected deformations are significant. Generally, the proposed workflow including the supervised point cloud matching ensures a high accuracy of the results.

5 Discussion

In this work, we introduced a pipeline for extending geodetic geo-monitoring networks by supervised point cloud matching. It allows the integration of point cloud data into a conventional rigorous deformation analysis, aiming to provide precise 3D vectors with significance information. Non-signalised virtual targets derived from laser scan patches using ICP matching improve the spatial resolution and the network geometry.

The selection of the patches plays a critical role in the methodology, ensuring that they are suitable for ICP matching. Our pipeline includes a quality assessment for each patch. The chosen threshold for filtering is a vital parameter, as it determines which patches contribute to the deformation analysis. Selecting a threshold near the measurement accuracy of the instrument ensures that the precision of observations in the network remains high.

Compared to feature-based approaches, filtering is not based on the local distribution of the resulting deformation vectors. In feature-based methods, false matches are often identified using histograms of the local neighbourhood, assuming that vectors in the spatial vicinity have a similar magnitude and direction. On the other hand, our proposed method analyses the selected structures already in advance, providing a robust mechanism for assessing the matching quality. Thus, it is not dependent on an assumption about the expected deformations, and even single points that move differently can be detected.

However, the selection process relies on sufficient geometric variation within structures. This limits the number of patches, using only part of the whole point cloud for deformation analysis. In cases where structures lack such variation or exhibit repeating geometries, no suitable structures may be identified. The number of patches is thus strongly dependent on the surface structure of the monitoring object. Rock faces typically provide enough structure. This might not be the case for other landslide objects. Additionally, the condition applies that no inner deformations occur within a patch, e.g. due to surface erosion. Not in all cases is this detectable within the MC simulation if there is nevertheless a clear local minimum to which the ICP converges. To improve this problem, either an additional threshold for the ICP residuals can be defined, or larger changes have to be pre-detected using the M3C2 algorithm, similar to how it is proposed in ref. [39].

The number of patches is also influenced by the spatial resolution of the scans. A higher resolution reveals more surface details, and thus, smaller and more unremarkable structures might be used. Together, the surface structure of the object and the scan resolution are the most determining factors for the patch size. For the rock face on Mt. Hochvogel and the used scan resolution of 1 cm we proposed a patch size of 30–50 cm. However, this might be entirely different for other applications and scanning setups. Generally, smaller patches help to increase the spatial resolution of the virtual points and reduce the risk of inner deformations within a scan.

The experimental validation demonstrates that the inclusion of virtual observations has the potential to improve the network geometry. The improved redundancy due to the additional virtual observations results in a more reliable and controllable network, enhancing the accuracy of the deformation analysis.

The real-world application on Mt. Hochvogel demonstrates that the methodology delivers accurate and reliable deformation vectors, even in challenging environmental conditions. We developed the method especially for this application, where only small movements occur and only in one direction. In the laboratory setup, however, we have shown that deformations in arbitrary directions could be detected with the same accuracy. In point-cloud-based monitoring, we often face the problem that deformations can only be revealed in a specific direction [7, 8]. Using suitable structures for ICP matching, however, we can detect out-of-plane and in-plane movements. Thus, the method is also suitable for more complex deformation processes.

Moreover, it is not limited to slow processes as long as the condition of no inner deformations is fulfilled, although

the epoch rate might have to be increased depending on the movement rate. However, this method is not conceptualised for larger and more sudden changes. In this case, other methods, such as the M3C2 algorithm, might be more suitable. Also, long-range applications are feasible. However, it is difficult to set up a decent network in this case. Still, the method can be applied to point clouds captured from only one station. Despite not having the advantages of a redundant network adjustment, the MC simulation still helps to select reliable patches.

6 Conclusion and outlook

The methodology presented in this study offers a promising approach to geodetic deformation monitoring, particularly in scenarios where conventional network-based monitoring alone may be insufficient. The hybrid approach combines the strengths of both point-based and point-cloud-based strategies. Point-based monitoring, with its established principles of redundancy and error propagation, offers a solid foundation for deformation analysis. However, network points are limited by environmental constraints, making it challenging to mark all critical points, especially in high-risk or inaccessible areas. On the other hand, point-cloud-based monitoring enhances spatial coverage and flexibility, allowing for detailed analysis of complex objects. This combination of network-based with patch-based strategies enhances the spatial resolution and the network geometry of the monitoring system, making it suitable for applications where precise 3D vectors with significance information are crucial, and not all network points can be marked.

Introducing a supervised selection process for patches based on a MC simulation ensures that only suitable structures are considered for ICP matching, thus preserving or even improving the network accuracy. Integrating all observations in a free network adjustment enables consistent error propagation and a trustworthy significance calculation for each point, facilitating a reliable interpretation of the monitoring results.

The experimental validation in both laboratory and real-world scenarios underscores the effectiveness of this approach. The ability to capture high-precision deformation vectors with significance information while also increasing spatial coverage enhances the capabilities of geodetic monitoring. Although at Mt. Hochvogel, the number of marked points is already high and may be sufficient to monitor the primary moving process, the extended method still helped to reveal more details. In future projects, no marked points could be used at all. This makes monitoring in dangerous and inaccessible areas much easier and more safe.

Currently, the method is limited by different factors that influence the number of potential patches and thus, the number of additional virtual points:

- the surface structure of the monitoring object
- the spatial resolution of the scans
- the patch size

The biggest limitation, however, is the manual preselection of potentially suitable patches. Due to the effort, it limits the number of proposed patches. However, supervised selection is a step toward automation. A fully automatic selection process will very likely increase the number of virtual points even more and help find patches on object surfaces with poor geometric variation. Several local features could be analysed to find possible candidates for patches, for example:

- local eigenvalue features
- the distribution of the local normal vectors
- the convex hull of a specific neighbourhood

In further research, we will look at the automation and the limiting factors mentioned above to further improve our method.

In summary, this methodology has the potential to advance geodetic monitoring in challenging and high-risk environments, contributing to improved risk prevention and enhanced understanding of deformation dynamics. The flexibility of the method is evident in its adaptability to different monitoring scenarios, including scanning total stations, laser scanners, or photogrammetry. This versatility makes it applicable across a wide range of use cases. Further research and practical applications will help refine and expand this approach for various geodetic monitoring scenarios.

Research ethics: Not applicable.
Author contributions: The authors have accepted responsibility for the entire content of this manuscript and approved its submission.
Competing interests: The authors state no conflict of interest.
Research funding: This research was done within the research project “AlpSenseRely” funded by the Bavarian State Ministry of the Environment and Consumer Protection (StMUV TUS01UFS-76976).
Data availability: Not applicable.

References

1. Huggel C, Clague JJ, Korup O. Is climate change responsible for changing landslide activity in high mountains? Earth Surf Process Landforms 2012;37:77—91.
2. Pelzer H. Zur Analyse geodätischer Deformationsmessungen [Reihe C: Dissertationen (164)]. München: Deutsche Geodätische Kommission bei der Bayerischen Akademie der Wissenschaften; 1971.
3. Zahs V, Hämmerle M, Anders K, Hecht S, Sailer R, Rutzinger M, et al. Multi—temporal 3D point cloud—based quantification and analysis of geomorphological activity at an alpine rock glacier using airborne and terrestrial LiDAR. Permafr Periglac Process 2019;30:222—38.
4. Schröder D, Anders K, Winiwarter L, Wujanz D. Permanent terrestrial LiDAR monitoring in mining, natural hazard prevention and infrastructure protection — chances, risks, and challenges: a case study of a rockfall in Tyrol, Austria. In: Proceedings of the 5th joint international symposium on deformation monitoring (JISDM). Valencia, Spain: Universitat Politècnica de València (UPV); 2022.
5. Kenner R, Gischig V, Gojcic Z, Quéau Y, Kienholz C, Figi D, et al. The potential of point clouds for the analysis of rock kinematics in large slope instabilities: examples from the Swiss Alps: Brinzauls, Pizzo Cengalo and Spitze Stei. Landslides 2022;39:80.
6. Tsakiri M, Lichti D, Pfeifer N. Terrestrial laser scanning for deformation monitoring. In: Proceedings of the 12th FIG symposium on deformation measurement and 3rd IAG symposium on geodesy for geotechnical and structural engineering. Baden, Austria; 2006.
7. Holst C, Kuhlmann H. Challenges and present fields of action at laser scanner based deformation analyses. J Appl Geodesy 2016;10:17—25.
8. Wunderlich T, Niemeier W, Wujanz D, Holst C, Neitzel F, Kuhlmann H. Areal deformation analysis from TLS point clouds — the challenge. Allg Vermessungs-Nachrichten (avn) 2016;123:340—51.
9. Wunderlich T, Raffl L, Wiedemann W. Creating identities — two solutions for rigorous deformation analysis of areal observations in engineering geodesy. Allg Vermessungs-Nachrichten (avn) 2020;127:61—8.
10. Heunecke O, Kuhlmann H, Welsch W, Eichhorn A, Neuner HB. Auswertung geodätischer Überwachungsmessungen, 2nd ed. Handbuch Ingenieurgeodäsie/Michael Möser/Gerhard Müller/Harald Schlemmer (Hrsg.). Berlin and Offenbach: Wichmann; 2013.
11. Kuhlmann H, Schwieger V, Wieser A, Niemeier W. Engineering geodesy — definition and core competencies. J Appl Geodesy 2014;8:327—34.
12. Lague D, Brodu N, Leroux J. Accurate 3D comparison of complex topography with terrestrial laser scanner: application to the Rangitikei canyon (N-Z). ISPRS J Photogrammetry Remote Sens 2013;82:10—26.
13. Winiwarter L, Anders K, Höfle B. M3C2-EP: pushing the limits of 3D topographic point cloud change detection by error propagation. ISPRS J Photogrammetry Remote Sens 2021;178:240—58.
14. Akca D. 3D modelling, texturing and applications in cultural heritage. In: Lecture notes for ISPRS WG VI/5 & summer school "Theory and Application of Laser Scanning." Ljubljana, Slovenia; 2007.
15. Ge X. Terrestrial laser scanning technology from calibration to registration with respect to deformation monitoring. Dissertation. Technical University of Munich, Germany; 2016.
16. Harmening C, Neuner H. Detecting rigid body movements from TLS-based areal deformation measurements. In: Proceedings of the 78th FIG working week 2016. Christchurch, New Zealand; 2016.
17. Holst C, Zeimetz P, Nothnagel A, Schauerte W, Kuhlmann H. Estimation of focal length variations of a 100-m radio telescope's main reflector by laser scanner measurements. J Survey Eng 2012;138:126—35.
18. Lindenbergh R, Pfeifer N. A statistical deformation analysis of two epochs of terrestrial laser data of a lock. In: Proceedings of the 7th conference on optical 3D measurement techniques. Vienna, Austria: TU Wien; 2005, II:61—70 pp.
19. Lindenbergh R, Uchanski L, Bucksch A, van Gosliga R. Structural monitoring of tunnels using terrestrial laser scanning. Rep Geodesy 2009;87:231—8.
20. Ohlmann-Bartusel J. Gaining areal deformations by using driving-attendant laser scanning for the new Austrian tunnelling method. In: Grün A, Kahmen H, editors. Optical 3-D measurement techniques IX. Vienna, Austria: TU Wien; 2009, II:20—8 pp.
21. Schäfer T, Weber T, Kyrinovic P, Zamecnikova M. Deformation measurement using terrestrial laser scanning at the hydropower station of Gabcikovo. In: Proceedings of INGEO 2004 and FIG regional Central and Eastern European conference on engineering surveying. Bratislava, Slovakia; 2004.
22. Raffl L, Wiedemann W, Wunderlich T. Non-signalized structural monitoring using scanning total stations. In: Proceedings of the 5th joint international symposium on deformation monitoring (JISDM). Athens, Greece; 2019.
23. Gojcic Z, Zhou C, Wieser A. Robust pointwise correspondences for point cloud based deformation monitoring of natural scenes. In: Proceedings of the 4th joint international symposium on deformation monitoring (JISDM). Athens, Greece; 2019.
24. Wagner A. A new approach for geo-monitoring using modern total stations and RGB+D images. Measurement 2016;82:64—74.
25. Holst C, Janßen J, Schmitz B, Blome M, Dercks M, Schoch-Baumann A, et al. Increasing spatio-temporal resolution for monitoring alpine solifluction using terrestrial laser scanners and 3D vector fields. Rem Sens 2021;13:1192.
26. Hosseini K, Reindl L, Raffl L, Wiedemann W, Holst C. 3D landslide monitoring in high spatial resolution by feature tracking and histogram analyses using laser scanners. Rem Sens 2024;16:138.
27. Yang Y, Schwieger V. Supervoxel-based targetless registration and identification of stable areas for deformed point clouds. J Appl Geodesy 2023;17:161—70.
28. Chmelina K, Jansa J, Hesina G, Traxler C. A 3-D laser scanning system and scan data processing method for the monitoring of tunnel deformations. J Appl Geodesy 2012;6:177—85.
29. Wujanz D. Terrestrial laser scanning for geodetic deformation monitoring. Dissertation. Berlin, Germany: Technische Universität Berlin; 2016, C.
30. Yang Y, Schwieger V. Patch-based M3C2: towards lower-uncertainty and higher-resolution deformation analysis of 3D point clouds. Int J Appl Earth Obs Geoinf 2023;125:103535. https://doi.org/10.1016/j.jag.2023.103535.
31. Besl PJ, McKay ND. Method for registration of 3-D shapes. In: Sensor fusion IV: control paradigms and data structures

international society for optics and photonics; 1992, vol 1611:586—607 pp.
32. Pfeiffer J, Zieher T, Bremer M, Wichmann V, Rutzinger M. Derivation of three-dimensional displacement vectors from multi-temporal long-range terrestrial laser scanning at the Reissenschuh landslide (Tyrol, Austria). Rem Sens 2018;10: 1688.
33. Frangez V, Serantoni E, Wieser A. Geodetic monitoring of digitally fabricated structures early after construction. In: Proceedings of the FIG working week 2020. Amsterdam, Netherlands; 2020: 10556 p.
34. Raffl L, Holst C. Including virtual target points from laser scanning into the point-wise rigorous deformation analysis at geo-monitoring applications. In: Proceedings of the 5th joint international symposium on deformation monitoring (JISDM). Valencia, Spain: Universitat Politècnica de València (UPV); 2022.
35. Li P, Wang R, Wang Y, Tao W. Evaluation of the ICP algorithm in 3D point cloud registration. IEEE Access 2020;8:68030—48.
36. Wujanz D. Araneo: Bestimmung eines erweiterten Unsicherheitsbudgets für die Deformationsmessung basierend auf terrestrischen Laserscans. Allg Vermessungs-Nachrichten (avn) 2019;126:53—63.
37. Ogundare JO. Precision surveying: the principles and geomatics practice. Hoboken: John Wiley and Sons Inc; 2016:293 ff. p.
38. Raffl L, Wunderlich T. Challenges and hybrid approaches in alpine rockslide prevention — an alarming case study. In: Proceedings of the 8th INGEO international conference on engineering surveying & 4th SIG symposium on engineering geodesy. online; 2020.
39. Lucks L, Stilla U, Hoegner L, Holst C. Photogrammetric rockfall monitoring in Alpine environments using M3C2 and tracked motion vectors. ISPRS Open J Photogrammetry Remote Sens 2024;12:100058. https://doi.org/10.1016/j.ophoto.2024.100058.